
CDG-MAE: Learning Correspondences from Diffusion Generated Views

Varun Belagali¹ Pierre Marza² Srikanth Yellapragada¹ Zilinghan Li³

Tarak Nath Nandi^{3,4} Ravi K Madduri^{3,4} Joel Saltz¹

Stergios Christodoulidis² Maria Vakalopoulou^{2,5} Dimitris Samaras¹

¹Stony Brook University ²MICS, CentraleSupélec, Université Paris-Saclay

³Argonne National Laboratory ⁴University of Chicago ⁵Archimedes/Athena RC

Abstract

Learning dense correspondences, critical for applications such as video label propagation, is hindered by tedious and unscalable manual annotation. Self-supervised methods address this by using a cross-view pretext task, often modeled with a masked autoencoder, where a masked target view is reconstructed from an anchor view. However, acquiring effective training data remains a challenge - collecting diverse video datasets is difficult and costly, while simple image crops lack necessary pose variations. This paper introduces CDG-MAE, a novel MAE-based self-supervised method that uses diverse synthetic views generated from static images via an image-conditioned diffusion model. These generated views exhibit substantial changes in pose and perspective, providing a rich training signal that overcomes the limitations of video and crop-based anchors. We present a quantitative method to evaluate local and global consistency of generated images, discussing their use for cross-view self-supervised pretraining. Furthermore, we enhance the standard single-anchor MAE setting to a multi-anchor strategy to effectively modulate the difficulty of the pretext task. CDG-MAE significantly outperforms state-of-the-art MAE methods reliant only on images and substantially narrows the performance gap to video-based approaches.

1 Introduction

Masked autoencoders (MAEs) learn rich visual representations by learning to reconstruct randomly masked parts of an image from the remaining visible context [16]. The paradigm of learning by reconstruction naturally extends to multi-view scenarios through cross-view correspondence learning [35, 36, 15, 11]. These methods exploit the redundancy in captured information and the inherent 3D consistency across viewpoints as strong cues for learning to model dynamics, physics and semantics. A specific adaptation, cross-view masked auto-encoding, tasks a model to reconstruct a masked view of a scene from another anchor view. By learning to complete missing parts of scene representations, cross-view masked auto-encoding leads to strong vision models capable of understanding underlying scene semantics.

Training vision models to learn correspondences requires capturing multiple images of the scene, which in the real world can be resource intensive. One common shortcut involves leveraging simulators to render diverse views of a scene [35, 36], but this is limited to static environments. To model motion and perspective changes, the data itself must exhibit dynamic changes. Collecting videos thus appears as a relevant alternative [15], but this comes with an acquisition cost as well as the more limited diversity of the scenes one can capture. For example, a video captures only a single motion scenario in a scene.

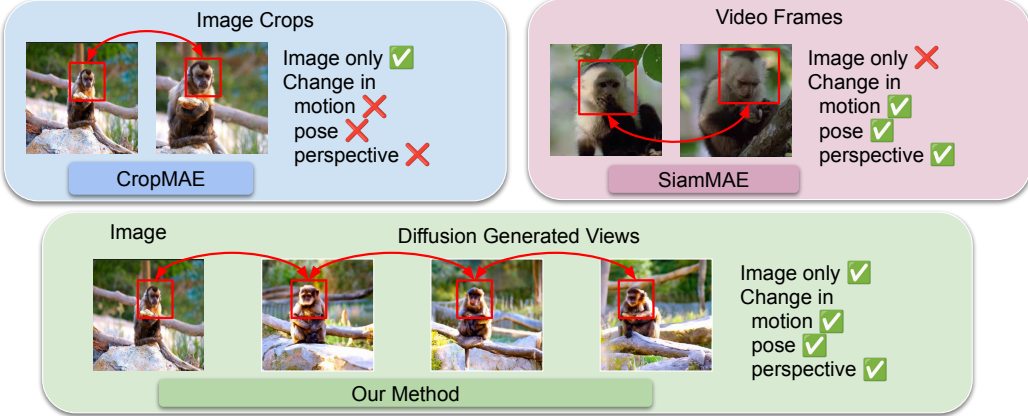


Figure 1: **CDG-MAE**: We train a vision encoder in a self-supervised manner by finding correspondences between real and synthetic views generated by a diffusion model. These synthetic views preserve important scene information while introducing diverse dynamics.

Given the large availability of 2D images, a natural question arises: can we generate dynamic variations from images equivalent to those found in videos for correspondence learning? A straightforward approach is to emulate changes with augmentations such as image crops [11], but the diversity of cropped views is limited. As acknowledged by [11], crops cannot introduce variations in pose, limiting the richness of learned inductive biases. Consequently, there is a need to develop methods that can use static images to derive richer, pose-variant transformations found in real-world dynamic scenes.

Diffusion models have shown strong performance in image generation [9, 29, 22], and can be controlled through various conditioning mechanisms to guide the generation process [29, 38]. Recent research focuses on conditioning diffusion models with image embeddings, enabling the generation of diverse variations of an input image in a self-supervised way [13, 23, 4]. Crucially, we observe that these variations can introduce different perspectives or diverse motion, equivalent to individual frames from a video (see Figure 1). However, for these to be used to learn correspondences, the generated views should introduce local changes while maintaining global consistency. Currently, quantitative tools to evaluate such properties have not been explored.

We thus present *CDG-MAE*, a cross-view self-supervised learning method to train Masked Autoencoders using views generated from a diffusion model. We employ an ImageNet-pretrained self-supervised diffusion model (S-LDM) from Gen-SIS [4], which uses image embeddings as the conditioning mechanism. We quantitatively assess the diversity of generated views, evaluating the local and global changes in images, demonstrating that the synthetic views introduce local changes in object poses and locations while maintaining global semantics. We then harvest the capabilities of this S-LDM to generate consistent views of an image with meaningful changes in pose and locations, providing rich training signal to the vision encoder without requiring video data. Finally, we extend the current single-anchor-view setting in cross-view self-supervised learning by using additional anchor views and applying an anchor-specific masking strategy to modulate the difficulty of the pretext task. Our contributions are as follows:

- (i) **Diffusion-based multi-view generation for MAE training.** We propose a novel way to train cross-view correspondence MAEs using the high quality signal coming from diverse views of scene with substantial changes in pose, generated from image conditioned diffusion models.
- (ii) **A new tool to evaluate cross-view consistency of view pairs of the same scene.** We develop a quantitative method to evaluate local and global consistency between two views. We demonstrate its use in evaluating pretraining data for self-supervised learning.

(iii) Multi-anchor masking as a novel MAE training paradigm. We extend the standard single-anchor MAE setting to a multi-anchor framework. Having multiple anchors allows for anchor masking, which creates a more challenging and effective pretext task.

We show that CDG-MAE, trained with diffusion-generated data and our multi-anchor setting, achieves substantial improvements over state-of-the-art MAE methods reliant on image crops and substantially narrows the performance gap with video-based approaches.

2 Related work

Self-supervised learning — Masked Image Modeling (MIM) is a self-supervised learning paradigm involving masking part of the input visual data and training models to predict these masked parts using visible parts [16, 2, 37, 34, 33, 1]. Specifically, Masked Autoencoders [16] (MAE) divide an image into patches, and mask some of these patches. An Encoder then processes only visible patches to extract features. These features are then appended with mask tokens that act as placeholders for masked patches. The encoder features and mask token with positional encoding are passed through the decoder that predicts the patch pixel values. With sufficiently high masking ratio, the encoder learns robust visual features that show strong performance on discriminative downstream tasks (classification, segmentation, object detection). Further, VideoMAE [33] extends MAE by pretraining on videos, integrating multiple frames. Even if, such an extension seems to be more informative, the requirement of videos for the pretraining could be costly. Apart from MAEs, there are also other style of SSL methods referred as view-invariant methods which use two augmentations of the same image, and train the model to match the global features between augmentations [6, 5, 14, 17] or additionally also match the local features [39, 25, 3]. In this work, we specifically focus on MAE as a self-supervised learning framework due to its efficiency, modularity, and popularity.

Cross-view self-supervised learning — aims at learning visual features that can be used to match cross-view features either for video [15, 11] or 3D [35, 36] downstream tasks. These works mainly employ Siamese style Masked Autoencoders to learn correspondences between views. The pretraining consists of two views: anchor and target. The target image is masked and passed through the encoder, and then a decoder is used to reconstruct the masked patches. The anchor view is also passed through the encoder independently without masking. To facilitate cross-view learning, the decoder reconstructs the target view by cross-attending to the encoder features of the anchor view. A high masking ratio ensures that the encoder learns features that can match patches of the anchor view to the target view. The difference in approaches mainly stems from the way the two views are derived. Siamese Masked Autoencoders [15] (SiamMAE) extracts target and anchor as two different frames of a video. Given that video consists of object motion, view point change, and pose change, SiamMAE learns strong visual features suitable for label propagation downstream tasks: video object propagation [27], semantic part propagation [40], and pose propagation [19]. Cropped Siamese Masked Autoencoder [11] (CropMAE) extends SiamMAE, where the two views are extracted from two crops of the same image, thus eliminating need of video data for pretraining. But, CropMAE performs subpar on challenging tasks like pose propagation, as the pretraining anchor and target views have limited changes in pose [11].

Diffusion models — can generate realistic images due to breakthroughs in conditioning mechanisms [18, 38], architecture [26, 10] and sampling techniques [30, 24]. Latent Diffusion Models [29] (LDM) train a diffusion model in compact VAE latent space instead of pixel space, hence making the training and generation more efficient. While diffusion models are commonly conditioned on explicit signals such as class labels and text captions, recent works [4, 23, 13] have explored training conditional diffusion models in a self-supervised manner. These approaches involve first training an image encoder using view-invariant self-supervised learning methods [5, 7] to learn robust image embeddings. The diffusion model is then conditioned on the output of the frozen encoder.

Diffusion models are increasingly utilized for data augmentation, especially within self-supervised setting. The authors of [31, 32] use large pre-trained models like Stable Diffusion to generate augmentations. In contrast, approaches like Gen-SIS [4] train the diffusion model on the same dataset used for the main SSL task. Aligning with our work’s emphasis on self-supervised learning, we use the ImageNet pretrained Diffusion model from [4] to generating diverse views for our experiments.

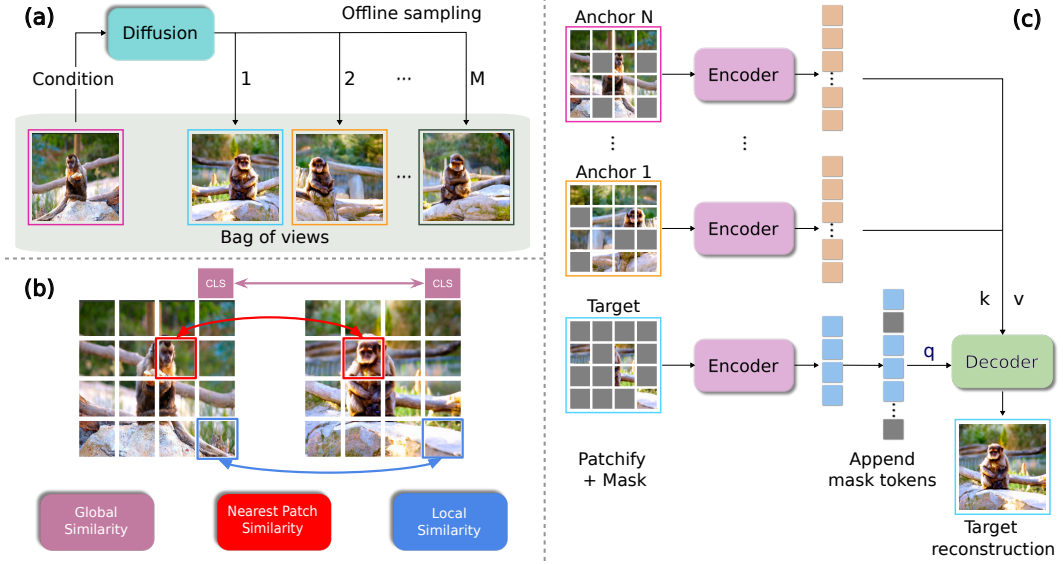


Figure 2: **Overview of CDG-MAE:** (a) For every real image, we generate M views using an off-the-shelf S-LDM [4]. (b) We develop a quantitative tool to evaluate local and global consistencies between view pairs. (c) We develop a multi-anchor framework to train cross-view MAE. Having multiple anchors allows for anchor masking, which creates a more challenging pretext task.

3 Method

Our approach, CDG-MAE, consists of three stages: 1) Bag of view generation. 2) Quantitative view evaluation and 3) cross-view MAE training. Figure 2 describes the overall pipeline of CDG-MAE.

3.1 Bag of views

Given an image-only dataset (ImageNet in our case), we generate M alternative views of the scene depicted by each real image via an off-the-shelf image-conditioned diffusion model. In this study, we use the ImageNet pre-trained diffusion model from [4] which was trained in a self-supervised fashion. Throughout the paper, we refer to this diffusion model as S-LDM (Self-supervised Latent Diffusion Model). S-LDM follows the Latent Diffusion Model [29] architecture and uses an image encoder as the conditioning network. The image encoder is pretrained using a view invariant SSL method [5] and frozen during the LDM training. We observe that S-LDM can generate diverse views of an input image with variations in motion, pose, and perspective, mimicking the changes between video frames, as seen in Figure 1. These M generated views, along with the original image, constitute the *bag of views* for that input, created offline to avoid online sampling during MAE training. Although bag of views incurs an overhead cost (135 ms per real image), it is still one-time cost as we sample offline before MAE-training.

3.2 Evaluating consistency between view pairs

Intuitively, an ideal pair of views (V_1, V_2) for correspondence learning should feature the same set of objects undergoing transformations in motion, pose, and perspective. Such views must therefore exhibit local variations that reflect these transformations while maintaining global consistency. To measure these properties, we developed an evaluation tool. Figure 2 (b) provides a visual illustration.

Let $f_*(\cdot)$ and $f_i(\cdot)$ denote functions that extract a transformer-based global and local embedding at a spatial location i , respectively for a single input V_1 . In our case, $f_*(V_1)$ is the $[CLS]$ token and $f_i(V_1)$ is the i^{th} patch token extracted from a ViT encoder. We use the pretrained ViT-B/16 MAE [16] to extract both patch tokens and CLS tokens. Let us assume there are L distinct spatial locations, indexed from 1 to L . Using this information we calculate the:

Global Similarity (GS) — Measures the overall semantic coherence between views V_1 and V_2 . It is defined as the cosine similarity ($sim(\mathbf{u}, \mathbf{v})$) between their respective global embeddings, $f_*(V_1)$ and $f_*(V_2)$. High GS is desirable, indicating that global semantic content is preserved.

Local Similarity (LS) — It is the average cosine similarity between local embeddings $f_i(V_1)$ and $f_i(V_2)$ from V_1 and V_2 respectively, at each identical spatial location i . A low LS can indicate changes in motion, pose, and perspective between views.

Nearest Patch Similarity (NPS) — Provides a measure of global consistency, especially in the presence of transformations. For each local embedding $f_i(V_1)$ in V_1 , we identify its nearest neighbor (most similar) among all local embeddings $\{f_j(V_2)\}_{j=1}^L$ from V_2 . NPS is then calculated as the average of these maximum similarity scores across all L locations in V_1 . Even with significant changes in motion, pose, or perspective, a high NPS is expected if the views remain globally coherent.

$$GS(V_1, V_2) = sim(f_*(V_1), f_*(V_2)) \quad (1)$$

$$LS(V_1, V_2) = \frac{1}{L} \sum_{i=1}^L sim(f_i(V_1), f_i(V_2)) \quad (2)$$

$$NPS(V_1, V_2) = \frac{1}{L} \sum_{i=1}^L \left(\max_{j \in \{1, \dots, L\}} sim(f_i(V_1), f_j(V_2)) \right) \quad (3)$$

Table 1 presents the evaluation from our quantitative tool of several types of view pairings: (i) video frames, (ii) synthetic views generated by the S-LDM, (iii) k-nearest neighbor (k-nn) image pairs from the training data, and (iv) random image pairs. The result demonstrates that S-LDM generated views are much closer to video frames than k-nn images or random pairs. This indicates that S-LDM, conditioned on static real images, can mimic characteristics of video data, making it ideal for correspondence learning.

Table 1: Quantitative evaluation of diffusion generated views when compared to video frames, k-nn images, and random pair of images. We sample random 500 images from ImageNet [8] and 500 pair of video frames from Kinetics-400 [21] for calculation.

Views	Global Sim. (\uparrow)	Local Sim. (\downarrow)	Nearest Patch Sim. (\uparrow)
Video frames	0.991	0.405	0.885
Diffusion (S-LDM)	0.991	0.384	0.794
K-nn images	0.955	0.310	0.722
Random images	0.894	0.181	0.605

3.3 CDG-MAE overall design and training strategy

In this section, we explain the overall design and training methodology for CDG-MAE: cross-view masked autoencoders using diffusion generated views. Consistent with existing works on cross-view MAE [15, 11], the pretext task is the reconstruction of randomly masked patches in a target, using visible target patches and anchor view. The architecture is an encoder-decoder Vision Transformer (ViT), where the target and each anchor are independently processed by a weight-shared ViT encoder. Subsequently, the decoder appends mask tokens to the visible target tokens, and reconstructs the content for these masked patches. This reconstruction is conditioned on visible target tokens through self-attention and on anchor tokens via cross-attention.

In the remainder of this section, we denote the encoder and decoder as e_θ and d_ψ respectively. We define image patchification operator as $\rho(\cdot)$, masking operator as $m(\cdot, \text{ratio})$, and concatenation as $[\cdot; \cdot]$. The masking ratios for the target and anchor views are denoted by r_t and r_a , respectively.

Encoding Target — The target image $T \in \mathbb{R}^{H \times W \times 3}$ is first patchified into a sequence of $N_t = (H/P) \times (W/P)$ non-overlapping patches, each of size $P \times P \times 3$. We then flatten these patches into a 1D sequence, and apply random masking using a high target masking ratio (r_t). We discard the masked patches \tilde{T}_v , and process the visible patches T_v through the encoder e_θ to obtain encoder target representations T'_v .

$$T_p = \rho(T), \quad T_v, \tilde{T}_v = m(T_p, r_t) \quad (4)$$

$$T'_v = e_\theta(m(T_p, r_t); \theta) \quad (5)$$

Multi-anchor and anchor-masking — Traditional cross-view MAEs such as SiamMAE [15] and CropMAE [11] typically encode a single unmasked anchor view. In CDG-MAE, we propose leveraging multiple anchor views, $\{A^k\}_{k=1}^N$, sampled from the "bag of views" (where N is the number of anchors). Furthermore, we introduce *anchor masking*: each anchor view A^k is independently masked with a specific anchor masking ratio (r_a), allowing for fine-grained control over the pretext task's difficulty. Higher N can provide the decoder with richer contextual information, simplifying target reconstruction. Conversely, applying anchor masking makes the task more challenging by reducing the visible information from each anchor. We demonstrate that an optimal balance between N and r_a enhances representation learning.

Similar to target encoding, each anchor A^k is patchified and masked. We discard masked anchor patches, and pass the visible patches through the weight-shared encoder e_θ (Siamese-style encoding) to obtain anchor tokens A'^k . We then concatenate the output tokens from all N anchors to form a aggregated anchor representation A'_v

$$A'^k = e_\theta(m(\rho(A^k), r_a); \theta), \quad \forall k \in \{1, \dots, N\} \quad (6)$$

$$A'_v = [A'^1_v; A'^2_v; \dots; A'^N_v] \quad (7)$$

Target reconstruction — The input to the decoder d_ψ is the sequence T_a , which is a concatenation of encoder target representations T'_v and mask tokens \tilde{T}_v . The decoder self-attends to all tokens within T_a , and cross-attends to the aggregated anchor representation A'_v , allowing it to leverage information across anchor views to predict the masked target patches. Our multi-anchor setting encourages the encoder e_θ to learn features that are robust for matching across a diverse set of views - beyond just two views as in prior work [16, 15, 11]. We apply reconstruction loss (MSE) between masked target patches \tilde{T}_v and decoder predictions T_r , following prior work [16, 15, 11].

$$T_a = [T'_v, \tilde{T}_v] \quad (8)$$

$$T_r = d_\psi(T_a, A'_v; \psi) \quad (9)$$

$$\mathcal{L}(T_r, T_p) = \frac{1}{|\tilde{T}_v|} \|T_r - \tilde{T}_v\|_2^2 \quad (10)$$

4 Experimental setting

Bag of Views creation — For real each image in the ImageNet-1K [8] training dataset, we generate $M = 4$ random synthetic views using the pretrained checkpoint of S-LDM [4]. The real image along with generated views are treated as the *bag of views*. The generation is done in offline mode and stored on the disk before training CDG-MAE. Following [4], we use a classifier-free guidance weight of 6 [18] and 50 DDIM [30] steps for sampling.

Training — We utilize the official codebase of CropMAE [11] and closely follow their setting. By default, we use a ViT-S/16 encoder and a four-layer decoder. Each decoder block has an embedding dimension of 256, and contains cross-attention, feedforward and self-attention modules. We train for 100 epochs on ImageNet-1K with a base learning rate of 1.5×10^{-4} and batch size of 2048.

From the *bag of views* (containing M views), one image is randomly chosen as the target and N additional images as anchors ($N < M$). We use a target masking ratio $r_a = 90\%$. In multi-anchor setting, we apply uniform anchor masking ratio across all anchors, with each anchor masked independently and randomly. We also investigate the impact of training with a reduced patch size by training both CropMAE and CDG-MAE with a ViT-S/8 backbones for 100 epochs. More training details are provided in supplementary.

Downstream evaluation — Following existing works [15, 11] we evaluate correspondence learning using three label propagation tasks in videos - 1) DAVIS-2017 [28] video object segmentation, 2) VIP

Table 2: It is optimal to choose real or generated image as the target view.

Target View	DAVIS $\mathcal{J} \& \mathcal{F}_m$	VIP mIoU	JHMDB PCK0.1
Always Real	61.3	37.1	46.8
Always Generated	60.0	37.1	46.5
Real or Generated	61.2	37.6	46.5
k-nn image	60.5	36.0	46.5

Table 3: A balanced target masking ratio ($r_t = 90\%$) yields best performance.

Masking Ratio (%)	DAVIS $\mathcal{J} \& \mathcal{F}_m$	VIP mIoU	JHMDB PCK0.1
75	60.0	34.9	46.2
90	61.2	37.6	46.5
98.5	60.7	35.5	44.4

[41] semantic part propagation, and 3) JHMDB [20] human pose propagation. In label propagation, we are provided the annotation of the first frame and the task is to propagate the label to all frames by computing similarity (correspondence) between patches of frames. The evaluation is done in a training-free manner using the pretrained encoder following the setting of [15, 11]. More details are provided in the supplementary.

5 Results

We first discuss the design choices of CDG-MAE in Sec 5.1, 5.2 and then compare with MAE-based methods in Sec 5.3. We also present results on training with smaller patch size in Sec 5.4.

5.1 Target selection and masking

To investigate the influence of target selection, we employ a simple single-anchor configuration where the anchor view is unmasked ($r_a = 0$) and a high target masking ratio ($r_t = 90\%$). We evaluate three strategies for selecting the target view: 1) always using the real image, 2) always using a diffusion-generated view or 3) random choice between real and generated. We observe in Table 2 that always using the real image as target and the random choice strategy yield comparable, strong performance. Hence, we adopt the random choice selection as the default strategy for CDG-MAE.

In Table 2, we also tested using k-nearest neighbor ($k = 5$) image pairs for anchor and target, and observe that it underperforms our default strategy. While k-nn images might share global feature similarity, Table 1 indicates they lack the high Nearest Patch Similarity found in video frames.

Next, in Table 3, we investigate the effect of target masking ratio (r_t). Unlike vanilla MAE (which uses $r_t = 75\%$), cross-view MAEs such as [11, 15] typically employ higher ratios ($\geq 90\%$). Lower ratios (e.g., 75%) can encourage the target to reconstruct itself, thereby hindering correspondence learning from anchor views. CropMAE uses a very high ratio ($r_t = 98.5\%$) to keep the task challenging under high information redundancy between anchor and target cropped from the same image. In CDG-MAE, such high ratio performs poorly. This can be attributed to the greater visual variations between diffusion generated anchor views and the target image compared to simple image crops. In our case, target reconstruction requires more context. We observe that a balanced masking ratio of $r_t = 90\%$ yields optimal performance.

5.2 Multi-anchor and anchor-masking

In this section, we explore the extension from a single-anchor to a multi-anchor framework. The latter enables us to introduce anchor masking, a technique not explored in prior methods such as SiamMAE [15] and CropMAE [11]. Table 4 demonstrates that transitioning from a single anchor to two anchors significantly improves performance across all datasets. With two anchors, the decoder can learn more robust correspondences by matching target patches across both views. Within the two-anchor configuration, applying an anchor masking ratio of 25% or 50% further enhances these results. Ultimately, we achieve optimal performance using three anchors with a 25% anchor masking ratio, as presented in Table 4. This highlights the need for anchor masking when increasing the number of anchors to avoid providing too much information to the decoder, which would greatly reduce task difficulty.

Table 4: Effect of multiple anchors and anchor masking (r_a). Multi-anchor training improves performance, and anchor masking offers control over pretext task difficulty. We report mean \pm std across 3 pretraining runs (seeds).

Num. of Anchors (N)	Anchor Masking ratio (r_a)	DAVIS $\mathcal{J} \& \mathcal{F}_m$	VIP mIoU	JHMDB PCK0.1
1	0	61.2 \pm 0.0	37.6 \pm 0.4	46.5 \pm 0.3
2	0	62.0 \pm 0.1	37.6 \pm 0.1	47.1 \pm 0.2
2	25%	62.4 \pm 0.2	38.0 \pm 0.3	47.3 \pm 0.1
2	50%	62.1 \pm 0.1	38.1 \pm 0.2	47.8 \pm 0.1
3	25%	62.6 \pm 0.1	38.1 \pm 0.1	47.8 \pm 0.2
3	50%	62.0 \pm 0.4	37.4 \pm 0.3	47.5 \pm 0.2

5.3 Comparison with other Masked Autoencoders

We compare CDG-MAE with several MAE baselines. These include vanilla MAE [16], video-based MAEs (Video-MAE [33] and MAE-ST [12]), and other cross-view MAEs such as CropMAE [11] and SiamMAE [15]. We evaluate two CDG-MAE variants: CDG-MAE-a1 (single unmasked anchor) and CDG-MAE-a3 (three anchors with 25% masking).

Results in Table 5 show that CDG-MAE significantly outperforms CropMAE across all downstream tasks, indicating the effectiveness of using diffusion generated views over crops of an image. See Figure 3 for a qualitative comparison. Furthermore, CDG-MAE-a3 achieves better performance than SiamMAE across most metrics. This is noteworthy because CDG-MAE is pretrained on the ImageNet-1K dataset, whereas SiamMAE is trained with video frames from Kinetics-400 dataset, and downstream evaluation tasks are video-based. This finding demonstrates the efficacy of our multi-anchor and anchor masking strategy for learning correspondences from static images.

Table 5: Comparison of CDG-MAE with other MAE based methods. a1 and a3 refer to single anchor and three anchors with 25% anchor masking respectively. \dagger refers to our reproduction on ImageNet-1K. The best and second-best results are highlighted in **Bold** and Underline.

Method	Arch	Dataset	Epochs	DAVIS			VIP mIoU	JHMDB	
				$\mathcal{J} \& \mathcal{F}_m$	\mathcal{J}_m	\mathcal{F}_m		PCK0.1	PCK0.2
SiamMAE [15]	ViT-S/16	Kinetics-400	2000	62.0	60.3	63.7	37.3	47.0	76.1
CropMAE \dagger [11]	ViT-S/16	ImagNet-1K	100	59.7	56.9	62.5	33.8	43.9	72.3
CDG-MAE-a1	ViT-S/16	ImagNet-1K	100	61.2	58.1	<u>64.3</u>	<u>37.6</u>	46.5	75.5
CDG-MAE-a3	ViT-S/16	ImagNet-1K	100	62.6	<u>59.7</u>	65.5	38.1	47.8	76.3
MAE [16]	ViT-B/16	ImagNet-1K	1600	53.5	52.1	55.0	28.1	44.6	73.4
Video-MAE [33]	ViT-S/16	Kinetics-400	800	39.3	39.7	38.9	23.3	41.0	67.9
MAE-ST [12]	ViT-L/16	Kinetics-400	800	54.6	55.5	53.6	33.2	44.4	72.5

5.4 Training with patch size 8

SiamMAE has demonstrated that reducing the encoder patch size from 16 to 8 can significantly enhance performance. At patch size 8, SiamMAE can learn more robust correspondences from fine-grained changes (variations of small objects) between two frames. We investigate the effect of smaller patch size for CDG-MAE, and compare with SiamMAE and CropMAE by training a ViT-S/8 encoder. Results are presented in Figure 4.

CropMAE shows no performance improvement with ViT-S/8 in object and part propagation. This is likely because cropped views lack sufficient fine-grained variations to benefit smaller patch training. In contrast, both SiamMAE and CDG-MAE exhibit notable performance gains with ViT-S/8 across all three tasks, compared to their ViT-S/16 variants. CDG-MAE significantly outperforms image-based CropMAE and closes the gap to the video-based SiamMAE. This highlights the ability of diffusion-generated views to provide diverse and rich variations beneficial for correspondence learning.

Furthermore, we evaluate the conditioning encoder of S-LDM [4] on these downstream tasks. As indicated by the dashed line in Figure 4, while this encoder performs adequately on object and

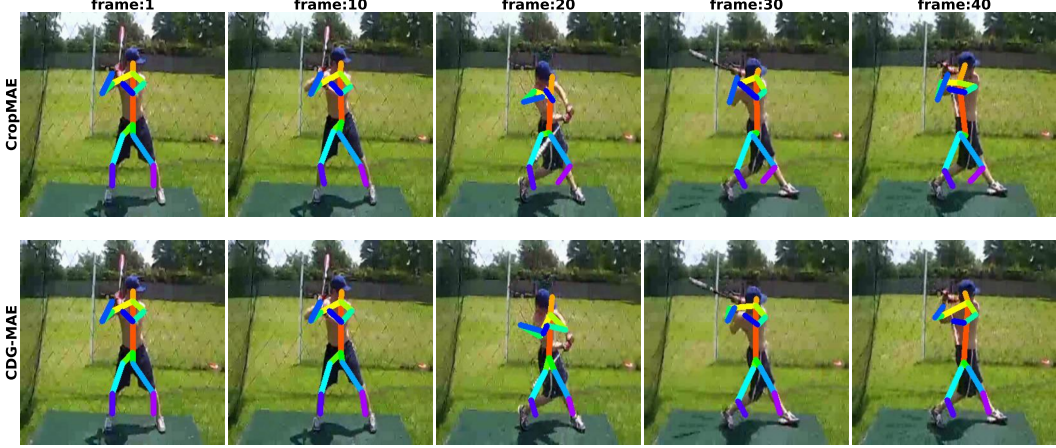


Figure 3: Visualization of pose propagation across frames (frame:1 is provided with ground-truth pose) using CropMAE and CDG-MAE on sample video in JHMDB dataset.

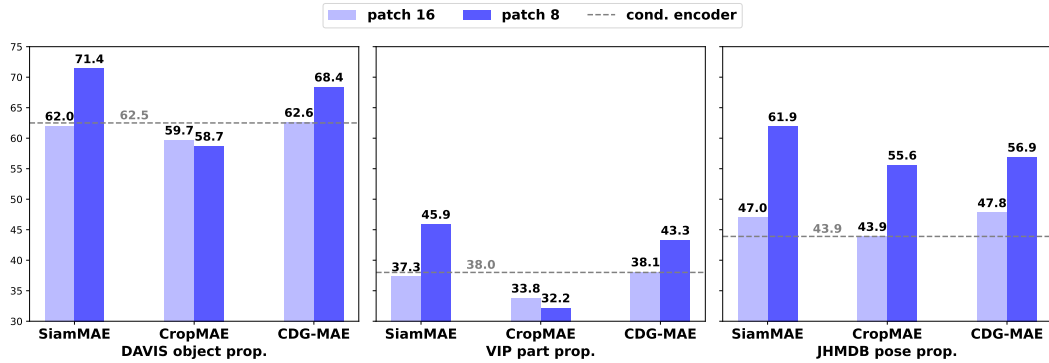


Figure 4: Performance of SiamMAE, CropMAE and CDG-MAE with ViT-S/16 and ViT-S/8 on DAVIS ($\mathcal{J} \& \mathcal{F}_m$), VIP (mIoU), and JHMDB (PCK0.1). We also present the performance of S-LDM’s conditioning encoder with a dashed line.

part propagation when compared to our ViT-S/16 encoder, it significantly underperforms in pose propagation. CDG-MAE ViT-S/8 outperforms the conditioning encoder in all three tasks. This shows that scaling tokens (patch size reduction) allows to better leverage diffusion-generated data, outperforming the original encoder used to condition the generation of such data.

6 Conclusion

We introduced CDG-MAE, a novel MAE framework for learning cross-view correspondence using diffusion-generated views. We developed a new quantitative tool to evaluate local and global consistency of generated views. Such properties, typically found in video data, are important to learn correspondences. CDG-MAE, trained with diffusion views derived from static images along, with our proposed multi-anchor masking, significantly outperforms existing crop-based MAE methods and substantially narrows the performance gap with video-based approaches. We hope our work inspires further exploration into synthetic data generation to leverage rich and diverse image datasets for cross-view representation learning.

Limitations and future work — Although self-supervised diffusion models can generate diverse variations needed for correspondence learning, we cannot control which specific variations occur between generated views. Future work can study how to better control variations, e.g. pose changes, in the generated views. This direction is challenging and interesting to explore as this should be done in a self-supervised way, i.e. without using pose labels.

7 Acknowledgments

This research has been supported by DATAIA international mobility scholarship, by the project MIS 5154714 of the National Recovery and Resilience Plan Greece 2.0 funded by the European Union under the NextGen-EU Program, NCI awards 1R21CA258493-01A1, 5U24CA215109, UH3CA225021, U24CA180924, NSF grants IIS-2123920, IIS-2212046, Stony Brook Profund 2022 seed funding, and generous support from Bob Beals and Betsy Barton. This research used resources of the Argonne Leadership Computing Facility, a U.S. Department of Energy (DOE) Office of Science user facility at Argonne National Laboratory and is based on research supported by the U.S. DOE Office of Science-Advanced Scientific Computing Research Program, under Contract No. DE-AC02-06CH11357.

References

- [1] M. Assran, Q. Duval, I. Misra, P. Bojanowski, P. Vincent, M. Rabbat, Y. LeCun, and N. Balas. Self-supervised learning from images with a joint-embedding predictive architecture. In *Proceedings of the IEEE/CVF Conference on Computer Vision and Pattern Recognition*, pages 15619–15629, 2023.
- [2] H. Bao, L. Dong, S. Piao, and F. Wei. Beit: Bert pre-training of image transformers. *arXiv preprint arXiv:2106.08254*, 2021.
- [3] A. Bardes, J. Ponce, and Y. LeCun. Vicregl: Self-supervised learning of local visual features. *Advances in Neural Information Processing Systems*, 35:8799–8810, 2022.
- [4] V. Belagali, S. Yellapragada, A. Graikos, S. Kapse, Z. Li, T. N. Nandi, R. K. Madduri, P. Prasanna, J. Saltz, and D. Samaras. Gen-sis: Generative self-augmentation improves self-supervised learning, 2024.
- [5] M. Caron, H. Touvron, I. Misra, H. Jégou, J. Mairal, P. Bojanowski, and A. Joulin. Emerging properties in self-supervised vision transformers. In *Proceedings of the IEEE/CVF international conference on computer vision*, pages 9650–9660, 2021.
- [6] T. Chen, S. Kornblith, M. Norouzi, and G. Hinton. A simple framework for contrastive learning of visual representations. In *International conference on machine learning*, pages 1597–1607. PMLR, 2020.
- [7] X. Chen, S. Xie, and K. He. An empirical study of training self-supervised vision transformers. In *Proceedings of the IEEE/CVF international conference on computer vision*, pages 9640–9649, 2021.
- [8] J. Deng, W. Dong, R. Socher, L.-J. Li, K. Li, and L. Fei-Fei. Imagenet: A large-scale hierarchical image database. In *2009 IEEE conference on computer vision and pattern recognition*, pages 248–255. Ieee, 2009.
- [9] P. Dhariwal and A. Nichol. Diffusion models beat gans on image synthesis. *Advances in neural information processing systems*, 34:8780–8794, 2021.
- [10] P. Esser, S. Kulal, A. Blattmann, R. Entezari, J. Müller, H. Saini, Y. Levi, D. Lorenz, A. Sauer, F. Boesel, D. Podell, T. Dockhorn, Z. English, K. Lacey, A. Goodwin, Y. Marek, and R. Rombach. Scaling rectified flow transformers for high-resolution image synthesis, 2024.
- [11] A. Eymaël, R. Vandeghen, A. Cioppa, S. Giancola, B. Ghanem, and M. Van Droogenbroeck. Efficient image pre-training with siamese cropped masked autoencoders. In *ECCV*, 2024.
- [12] C. Feichtenhofer, Y. Li, K. He, et al. Masked autoencoders as spatiotemporal learners. *Advances in neural information processing systems*, 35:35946–35958, 2022.
- [13] A. Graikos, S. Yellapragada, M.-Q. Le, S. Kapse, P. Prasanna, J. Saltz, and D. Samaras. Learned representation-guided diffusion models for large-image generation. In *Proceedings of the IEEE/CVF Conference on Computer Vision and Pattern Recognition (CVPR)*, pages 8532–8542, June 2024.

[14] J.-B. Grill, F. Strub, F. Altché, C. Tallec, P. Richemond, E. Buchatskaya, C. Doersch, B. Avila Pires, Z. Guo, M. Gheshlaghi Azar, et al. Bootstrap your own latent-a new approach to self-supervised learning. *Advances in neural information processing systems*, 33:21271–21284, 2020.

[15] A. Gupta, J. Wu, J. Deng, and F.-F. Li. Siamese masked autoencoders. *NeurIPS*, 2023.

[16] K. He, X. Chen, S. Xie, Y. Li, P. Dollár, and R. Girshick. Masked autoencoders are scalable vision learners. In *Proceedings of the IEEE/CVF conference on computer vision and pattern recognition*, pages 16000–16009, 2022.

[17] K. He, H. Fan, Y. Wu, S. Xie, and R. Girshick. Momentum contrast for unsupervised visual representation learning. In *Proceedings of the IEEE/CVF conference on computer vision and pattern recognition*, pages 9729–9738, 2020.

[18] J. Ho and T. Salimans. Classifier-free diffusion guidance. *arXiv preprint arXiv:2207.12598*, 2022.

[19] H. Jhuang, J. Gall, S. Zuffi, C. Schmid, and M. J. Black. Towards understanding action recognition. In *Proceedings of the IEEE international conference on computer vision*, pages 3192–3199, 2013.

[20] H. Jhuang, J. Gall, S. Zuffi, C. Schmid, and M. J. Black. Towards understanding action recognition. In *Proceedings of the IEEE international conference on computer vision*, pages 3192–3199, 2013.

[21] W. Kay, J. Carreira, K. Simonyan, B. Zhang, C. Hillier, S. Vijayanarasimhan, F. Viola, T. Green, T. Back, P. Natsev, et al. The kinetics human action video dataset. *arXiv preprint arXiv:1705.06950*, 2017.

[22] B. F. Labs. Flux. <https://github.com/black-forest-labs/flux>, 2024.

[23] T. Li, D. Katabi, and K. He. Return of unconditional generation: A self-supervised representation generation method. *Advances in Neural Information Processing Systems*, 37:125441–125468, 2024.

[24] C. Lu, Y. Zhou, F. Bao, J. Chen, C. Li, and J. Zhu. Dpm-solver++: Fast solver for guided sampling of diffusion probabilistic models, 2023.

[25] M. Oquab, T. Darcet, T. Moutakanni, H. Vo, M. Szafraniec, V. Khalidov, P. Fernandez, D. Haziza, F. Massa, A. El-Nouby, et al. Dinov2: Learning robust visual features without supervision. *arXiv preprint arXiv:2304.07193*, 2023.

[26] W. Peebles and S. Xie. Scalable diffusion models with transformers. In *Proceedings of the IEEE/CVF international conference on computer vision*, pages 4195–4205, 2023.

[27] J. Pont-Tuset, F. Perazzi, S. Caelles, P. Arbeláez, A. Sorkine-Hornung, and L. Van Gool. The 2017 davis challenge on video object segmentation. *arXiv preprint arXiv:1704.00675*, 2017.

[28] J. Pont-Tuset, F. Perazzi, S. Caelles, P. Arbeláez, A. Sorkine-Hornung, and L. Van Gool. The 2017 davis challenge on video object segmentation. *arXiv preprint arXiv:1704.00675*, 2017.

[29] R. Rombach, A. Blattmann, D. Lorenz, P. Esser, and B. Ommer. High-resolution image synthesis with latent diffusion models. In *Proceedings of the IEEE/CVF conference on computer vision and pattern recognition*, pages 10684–10695, 2022.

[30] J. Song, C. Meng, and S. Ermon. Denoising diffusion implicit models. *arXiv preprint arXiv:2010.02502*, 2020.

[31] Y. Tian, L. Fan, K. Chen, D. Katabi, D. Krishnan, and P. Isola. Learning vision from models rivals learning vision from data. In *Proceedings of the IEEE/CVF conference on computer vision and pattern recognition*, pages 15887–15898, 2024.

[32] Y. Tian, L. Fan, P. Isola, H. Chang, and D. Krishnan. Stablerep: Synthetic images from text-to-image models make strong visual representation learners. *Advances in Neural Information Processing Systems*, 36, 2024.

[33] Z. Tong, Y. Song, J. Wang, and L. Wang. Videomae: Masked autoencoders are data-efficient learners for self-supervised video pre-training. *Advances in neural information processing systems*, 35:10078–10093, 2022.

[34] C. Wei, H. Fan, S. Xie, C.-Y. Wu, A. Yuille, and C. Feichtenhofer. Masked feature prediction for self-supervised visual pre-training. In *Proceedings of the IEEE/CVF conference on computer vision and pattern recognition*, pages 14668–14678, 2022.

[35] P. Weinzaepfel, V. Leroy, T. Lucas, R. Brégier, Y. Cabon, V. Arora, L. Antsfeld, B. Chidlovskii, G. Csurka, and J. Revaud. Croco: Self-supervised pre-training for 3d vision tasks by cross-view completion. *NeurIPS*, 2022.

[36] P. Weinzaepfel, T. Lucas, V. Leroy, Y. Cabon, V. Arora, R. Brégier, G. Csurka, L. Antsfeld, B. Chidlovskii, and J. Revaud. Croco v2: Improved cross-view completion pre-training for stereo matching and optical flow. In *ICCV*, 2023.

[37] Z. Xie, Z. Zhang, Y. Cao, Y. Lin, J. Bao, Z. Yao, Q. Dai, and H. Hu. Simmim: A simple framework for masked image modeling. In *Proceedings of the IEEE/CVF conference on computer vision and pattern recognition*, pages 9653–9663, 2022.

[38] L. Zhang, A. Rao, and M. Agrawala. Adding conditional control to text-to-image diffusion models. In *Proceedings of the IEEE/CVF international conference on computer vision*, pages 3836–3847, 2023.

[39] J. Zhou, C. Wei, H. Wang, W. Shen, C. Xie, A. Yuille, and T. Kong. ibot: Image bert pre-training with online tokenizer. *arXiv preprint arXiv:2111.07832*, 2021.

[40] Q. Zhou, X. Liang, K. Gong, and L. Lin. Adaptive temporal encoding network for video instance-level human parsing. In *Proceedings of the 26th ACM international conference on Multimedia*, pages 1527–1535, 2018.

[41] Q. Zhou, X. Liang, K. Gong, and L. Lin. Adaptive temporal encoding network for video instance-level human parsing. In *Proceedings of the 26th ACM international conference on Multimedia*, pages 1527–1535, 2018.

A Appendix

A.1 Implementation details

A.1.1 Training

Our implementation is built using the CropMAE [11] codebase. We use ImageNet-1K as our pretraining dataset. The default training hyperparameters for our method (CDG-MAE) under the single anchor setting are presented in Table 6. We also provide the hyperparameters of CropMAE as a reference. CDG-MAE also uses cropping as an augmentation, following SiamMAE [15].

A.1.2 Downstream Evaluation

We evaluate our method on standard video label propagation tasks, following the evaluation protocol of previous works [11, 15]. We use three datasets: 1) DAVIS [27] for video object segmentation, 2) VIP [40] for semantic part propagation, and 3) JHMDB [19] for human pose propagation. In these tasks, annotation is provided for the first frame, and the objective is to propagate ground-truth labels to all subsequent frames of the video.

The evaluation is performed in a training-free manner using k -nearest neighbor (k -NN) inference. Furthermore, this protocol utilizes a memory queue of the last few frames and restricts source patches to the query’s spatial neighborhood. The specific hyperparameter values for this setup are detailed in Table 7.

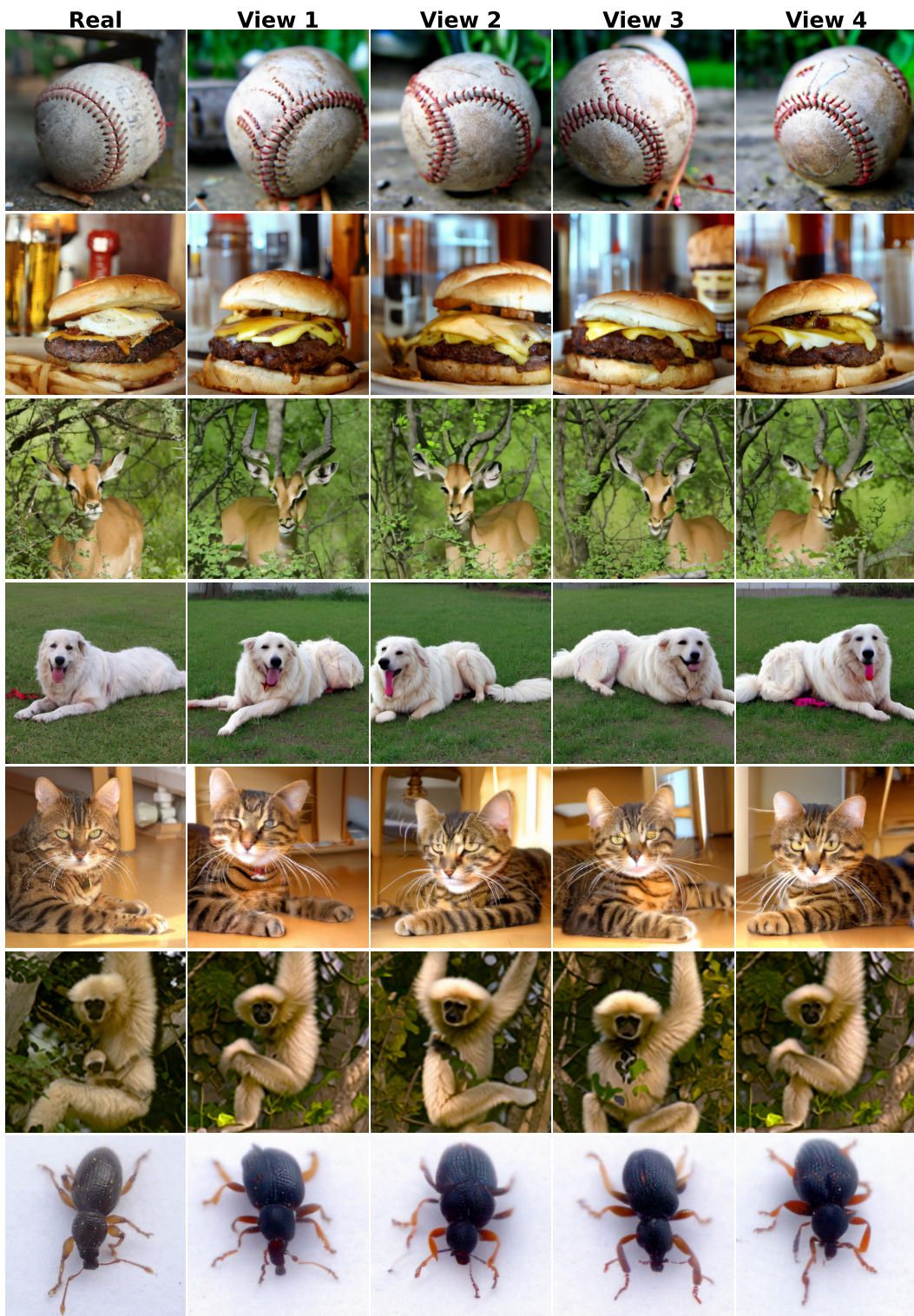


Figure 5: Bag of views visualization. Real denotes an image in ImageNet dataset. The views represent the synthetic views generated with diffusion.

Table 6: Training hyperparameters for CDG-MAE and CropMAE [11]

	CDG-MAE (ours)	CropMAE
Optimizer	AdamW ($\beta_1=0.9, \beta_2=0.95$)	AdamW ($\beta_1=0.9, \beta_2=0.95$)
Weight decay	0.05	0.05
Base learning rate	1.5×10^{-4}	1.5×10^{-4}
Target masking ratio	90%	98.5%
<i>lr</i> schedule	Cosine Decay	Cosine Decay
Epochs	100	100
Batch size	2048	2048
Bag of views size (M)	4	—
Augmentations	Crop [0.5, 1.0] (0.75, 1.33)	LocalToGlobal Crop [(0.3, 6.0) (0.1, 1.0)] (0.75, 1.33)
Aspect ratio		

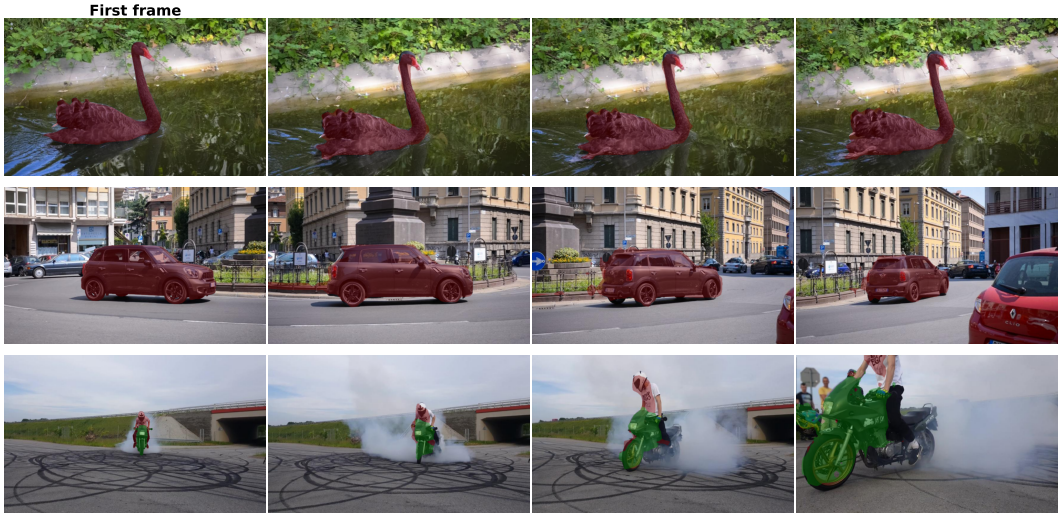


Figure 6: Visualization of label propagation using CDG-MAE ViT-S/16 on DAVIS [27] dataset. The first frame is annotated with the ground truth object segmentation masks.



Figure 7: Visualization of label propagation using CDG-MAE ViT-S/16 on VIP [40] dataset. The first frame is annotated with the semantic part segmentation masks.

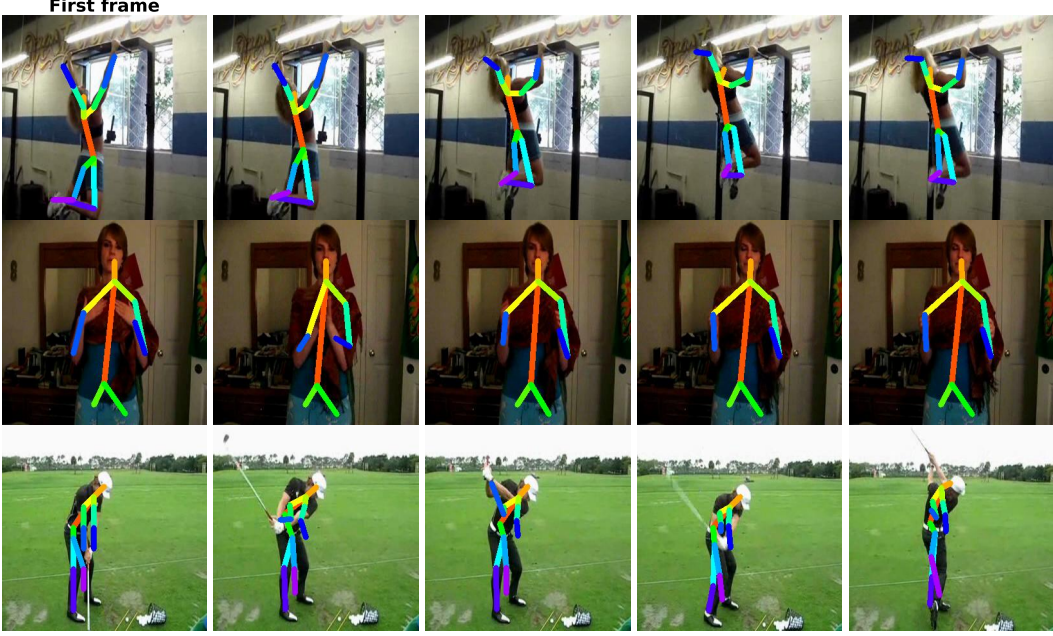


Figure 8: Visualization of label propagation using CDG-MAE ViT-S/16 on JHMDB [19] dataset. The first frame is annotated with the pose labels.

For DAVIS, we report mean region similarity (\mathcal{J}_m), mean contour accuracy (\mathcal{F}_m), and their combined average ($\mathcal{J} \& \mathcal{F}_m$). For VIP, we report the mean Intersection over Union (mIoU). For JHMDB, evaluation is based on PCK0.1 and PCK0.2, which represent the percentage of keypoints correctly localized within an error margin of 10% and 20% of the bounding box size, respectively. We use the evaluation codebase released by CropMAE [11].

Table 7: Hyperparameters for downstream evaluation using k -nearest neighbor (k -NN) inference.

	DAVIS	VIP	JHMDB
Top-K	7	10	7
Queue Length	20	20	20
Neighborhood Size	20	20	20

A.2 Visualization

Figure 5 shows samples from the bag of views generated using the ImageNet-1K dataset. As seen in the figure, the views exhibit changes in pose, motion, and perspective. Moreover, one can observe that the generated images maintain the main characteristics of the image (objects and background) making them ideal for the training of our CDG-MAE method.

Qualitative results of CDG-MAE on downstream tasks are presented in Figure 6, Figure 7, and Figure 8.

A.3 Computation analysis

A.3.1 Multi-anchor and anchor masking

Table 4 in main paper shows that using multiple anchors with anchor masking improves downstream task performance. In this section and Table 8, we discuss the associated training computational complexity (evaluation-time inference complexity is the same for all models). GLOPs are calculated using a full forward pass up to the loss calculation with a single input training sample. Adding more anchors without anchor masking increases the computational complexity as it results in more tokens being processed by the encoder and decoder. However, introducing anchor masking not only

improves performance, but can also help in reducing GLOPs. This is since the masked tokens are dropped at the input and hence do not add complexity, effectively decreasing the number of tokens processed by the encoder for each anchor, and finally the number of tokens used in cross-attention by the decoder. As presented in Table 8, $N = 2$ anchors and $r_a = 50\%$ can maintain almost the same number of FLOPs as the single-anchor setting and outperforms it in downstream tasks. Further, to make the most out of multiple anchors, our best model uses $N = 3$ anchors and $r_a = 25\%$. Finally, for $N = 4$ we noticed no further improvement and even a small decrease in performance. For this reason, we performed only one seed run for $N = 4$.

Table 8: Extension of Table 4 in main paper with GLOPs: Effect of multiple anchors and anchor masking (r_a). Multi-anchor training improves performance, and anchor masking offers control over pretext task difficulty, along with reducing training-time computational complexity.

Num. of Anchors (N)	Anchor Masking ratio (r_a)	DAVIS $\mathcal{J} & \mathcal{F}_m$	VIP mIoU	JHMDB PCK0.1	GFLOPs
1	0	61.2 ± 0.0	37.6 ± 0.4	46.5 ± 0.3	6.0
2	0	62.0 ± 0.1	37.6 ± 0.1	47.1 ± 0.2	10.4
2	25%	62.4 ± 0.2	38.0 ± 0.3	47.3 ± 0.1	8.3
2	50%	62.1 ± 0.1	38.1 ± 0.2	47.8 ± 0.1	6.1
3	25%	62.6 ± 0.1	38.1 ± 0.1	47.8 ± 0.2	11.6
3	50%	62.0 ± 0.4	37.4 ± 0.3	47.5 ± 0.2	8.3
4	25%	62.3	37.6	47.6	14.9
4	50%	61.7	37.4	47.6	10.6

A.3.2 Bag of views

For each training image in ImageNet-1K (1.28 M images), we generate 4 synthetic views and store them on disk. The total computation cost for the creation of bag of views on a single node of 8 A100 GPUs is approximately 48 hrs and it is performed only once.

A.3.3 Machine details and total budget

We use a single node with 8 A100 40 GB GPUs for all the experiments. The CDG-MAE ViT-S/16 model takes a maximum of 14 hours for training. A total of 900 node hours was used for this paper including the initial exploration and failed experiments.

A.4 Additional experiments

A.4.1 Choice of diffusion model

In the literature, there are two ImageNet-1K diffusion models pretrained in a self-supervised way (S-LDMs): Gen-SIS [4] and RCG [23]. We opted to use the S-LDM from Gen-SIS based on the quantitative metrics we introduce in the main paper. Indeed, Table 9 shows that views generated from the S-LDM from Gen-SIS are considerably closer to video frames. We also trained CDG-MAE with views from the S-LDM from RCG and found its performance to be inferior to that achieved with the S-LDM from Gen-SIS (Table 10). This finding further underscores the importance of our proposed metrics in identifying the optimal views needed for learning correspondence.

Table 9: Quantitative evaluation of diffusion-generated views when compared to video frames. We sample random 500 images from ImageNet [8] and 500 pair of video frames from Kinetics-400 [21] for calculation.

Views	Global Sim. (\uparrow)	Local Sim. (\downarrow)	Nearest Patch Sim. (\uparrow)
Video frames	0.991	0.405	0.885
Gen-SIS S-LDM	0.991	0.384	0.794
RCG S-LDM	0.951	0.299	0.735

Table 10: Downstream evaluation of CDG-MAE when trained with views from Gen-SIS S-LDM vs RCG S-LDM. We use the single anchor setting for this comparison.

Views	DAVIS	VIP	JHMDB
	$\mathcal{J} \& \mathcal{F}_m$	mIoU	PCK0.1
Gen-SIS S-LDM	61.2	37.6	46.5
RCG S-LDM	57.4	34.8	43.7

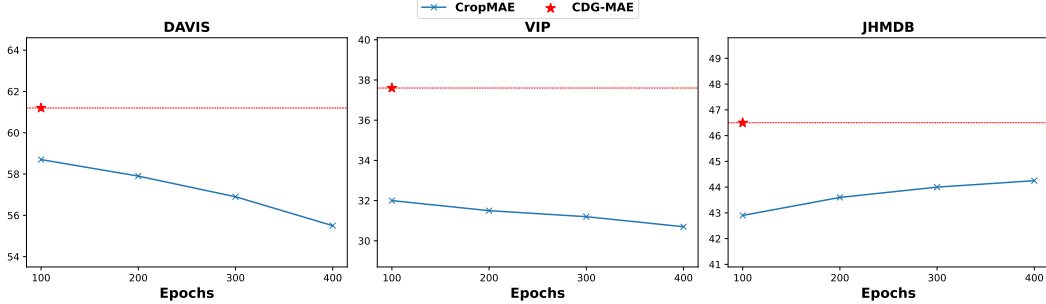


Figure 9: Performance of CropMAE when trained with 400 epochs schedule. We report the evaluation on DAVIS ($\mathcal{J} \& \mathcal{F}_m$), VIP (mIoU), and JHMDB (PCK0.1). We also present the performance of CDG-MAE trained for 100 epochs with single anchor setting.

A.4.2 Training CropMAE with more epochs

We compare the performance of CDG-MAE trained for 100 epochs with CropMAE trained for longer schedule (400 epochs). As studied by CropMAE [11] paper, extended training might lead to saturation in performance. In Figure 9, we observe the similar trend, where the performance of CropMAE starts to decrease on DAVIS and VIP, and saturates on the JHMDB dataset. CDG-MAE trained with 100 epochs can outperform CropMAE even when CropMAE is trained for longer.